We are concerned here with the determination of a_{mn} and b_{mn}. By evaluating the volume integral of

$$\nabla\cdot(\overline{E}_{mn}^{+}\times\overline{H}-\overline{E}\times\overline{H}_{mn}^{+}) \tag{27}$$

over the volume bounded by S_1, S_2 and the guide walls, and by applying the divergence theorem, one obtains

$$\int_{S_1+S_2}(\overline{E}_{mn}^{+}\times\overline{H}-\overline{E}\times\overline{H}_{mn}^{+})dS = -\int_V j\omega\mu_0\overline{m}\cdot\overline{H}_{mn}^{+}\,dV. \tag{28}$$

The first integral is over S_1+S_2 only, because of the boundary condition at the metal walls, and the second integral is over V only, since $\overline{m}=0$ outside V.

Using (24) and (25) when integrating over S_2 and S_1, respectively, and observing relations (23), and (28) yields

$$2b_{mn}=\int_V j\omega\mu_0\overline{m}\cdot\overline{H}_{mn}^{+}\,dV. \tag{29}$$

If $\overline{E}_{mn}^{+}$ and $\overline{H}_{mn}^{+}$ are substituted by $\overline{E}_{mn}^{-}$ and $\overline{H}_{mn}^{-}$ in (28), one would obtain in the same fashion

$$2a_{mn}=\int_V j\omega\mu_0\overline{m}\cdot\overline{H}_{mn}^{-}\,dV. \tag{30}$$

We are interested in the transverse components of the total $\overline{E}^{\pm}$. They are given by

$$\overline{E}_{tmn}^{\pm}=\sum_{mn}\left[\pm\frac{1}{2}j\omega\mu_0\int_V\overline{m}\cdot\bar{h}_{tmn}dV\right]\bar{e}_{tmn}e^{\pm\Gamma_{mn}z}. \tag{31}$$

ACKNOWLEDGMENT

The author wishes to thank Prof. M. Chodorow and Dr. H. J. Shaw of Stanford Microwave Laboratory for supervising this work. Thanks are also due to Gwen Good for her calculations.

REFERENCES

[1] J. C. Sethares and S. J. Naumann, "Design of microwave dielectric resonators," *IEEE Trans. Microwave Theory and Techniques*, vol. MTT-14, pp. 2–7, January 1966.
[2] A. Okaya and L. F. Barash, "The dielectric microwave resonator," *Proc. IRE*, vol. 50, pp. 2081–2092, October 1962.
[3] H. Y. Yee, "An investigation of microwave dielectric resonators," Microwave Laboratory, Stanford University, Stanford, Calif., Rept. M. L. 1065, July 1963.
[4] ——, "Natural resonant frequencies of microwave dielectric resonators," *IEEE Trans. Microwave Theory and Techniques*, vol. MTT-13, p. 256, March 1965.
[5] A. Karp, H. J. Shaw, and D. K. Winslow, "Circuit properties of microwave dielectric resonators," *IEEE Trans. Microwave Theory and Techniques*, vol. MTT-16, pp. 818–828, October 1968.
[6] R. E. Collin, *Field Theory of Guided Waves*. New York: McGraw-Hill, 1960, pp. 200–204.
[7] S. B. Cohn, "Microwave bandpass filters containing high Q dielectric resonators," *IEEE Trans. Microwave Theory and Techniques*, vol. MTT-16, pp. 218–227, April 1968.
[8] E. G. H. Lean, "Studies of microwave shear waves in solids," Microwave Laboratory, Stanford University, Stanford, Calif., Rept. M.L. 1543, May 1967.
[9] J. A. Kusters, "Acoustic delay line application of microwave dielectric resonators," in preparation.

Slot Line on a Dielectric Substrate

SEYMOUR B. COHN, FELLOW, IEEE

Abstract—**Slot line consists of a narrow gap in a conductive coating on one side of a dielectric substrate, the other side of the substrate being bare. If the substrate's permittivity is sufficiently high, such as $\varepsilon_r=10$ to 30, the slot-mode wavelength will be much smaller than free-space wavelength, and the fields will be closely confined near the slot. Possible applications of slot line to filters, couplers, ferrite devices, and circuits containing semiconductor elements are discussed. Slot line can be used either alone or with microstrip line on the opposite side of the substrate. A "second-order" analysis yields formulas for slot-line wavelength, phase velocity, group velocity, characteristic impedance, and effect of adjacent electric and magnetic walls.**

Manuscript received February 17, 1969; revised May 15, 1969. This work was performed for Stanford Research Institute as a part of their study program for U. S. Army Electronics Command, Contract DAAB07-68-c-0088. This paper covers material presented at the 1968 G-MTT Symposium, Detroit, Mich., May 20–22, 1968.

The author is a consultant to Stanford Research Institute, Menlo Park, Calif.

I. INTRODUCTION

SLOT LINE consists of a slot or gap in a conductive coating on a dielectric substrate, as shown in Fig. 1. Both resonant and propagating slots in metal sheets have been used as radiating antenna elements (see [1], [2], and [3], and their bibliographies). For slot line to be practical as a transmission line, radiation must be minimized. This is accomplished through the use of a high permittivity substrate, which causes the slot-mode wavelength λ' to be small compared to free-space wavelength λ, and thereby results in the fields being closely confined to the slot with negligible radiation loss. For example, if $\epsilon_r=20$, then $\lambda'/\lambda\approx\frac{1}{3}$, and analysis shows the slot-mode fields to be sharply attenuated at a distance $r/\lambda=\frac{1}{8}$, or $r=0.5$ inch at 3 GHz.

Fig. 2(a) shows the slot-mode fields in a cross-sectional view. A voltage difference exists between the slot edges. The

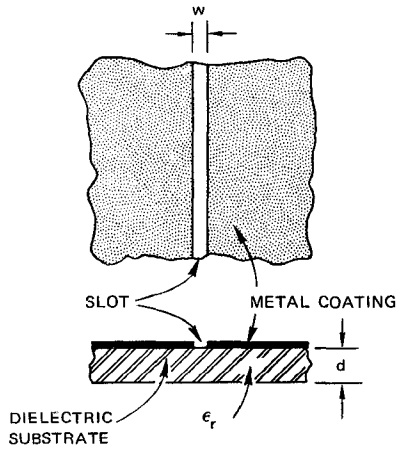

Fig. 1. Slot line on a dielectric substrate.

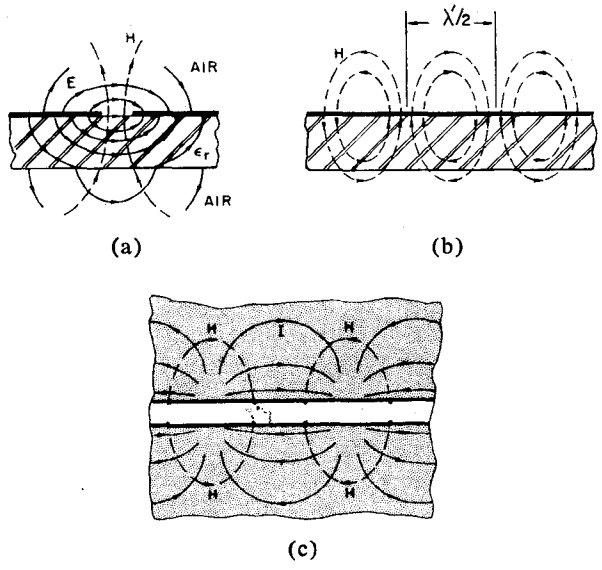

Fig. 2. Field and current distribution. (a) Field distribution in cross section. (b) H field in longitudinal section. (c) Current distribution on metal surface.

electric field extends across the slot; the magnetic field is perpendicular to the slot. Because the voltage occurs across the slot, the configuration is especially convenient for connecting shunt elements such as diodes, resistors, and capacitors. The longitudinal view in Fig. 2(b) shows that in the air regions the magnetic field lines curve and return to the slot at half-wavelength intervals. Consequently, a propagating wave has elliptically polarized regions that can be usefully applied in creating certain ferrite components. The current paths on the conducting surface are shown in Fig. 2(c). The surface-current density is greatest at the edges of the slot and decreases rapidly with distance from the slot. A propagating wave has regions of elliptically polarized current and magnetic field in this view, also.

An interesting possibility for microwave integrated circuits is the use of slot lines on one side of a substrate and microstrip lines on the other. When close to each other, coupling between the two types of lines will exist, and when sufficiently far apart they will be independent. Coupling between a slot

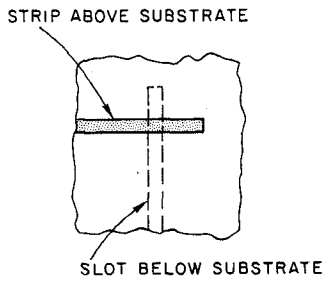

Fig. 3. Simple transition between slot line and microstrip.

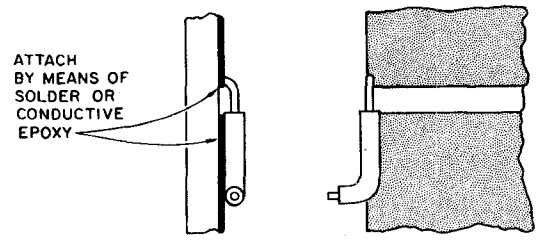

Fig. 4. Broad-band transition between slot line and miniature semirigid coaxial line.

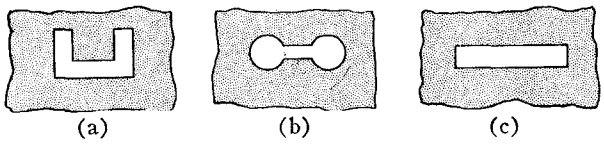

Fig. 5. Resonant slots.

and a strip can be used intentionally in certain components. For example, parallel lengths of slot and strip can be made to act as a directional coupler. If a slot and strip cross each other at right angles, as in Fig. 3, coupling will be especially tight, and a transition covering approximately 30-percent bandwidth can be achieved when the strip and slot widths are optimally related, and when the strip and slot are extended approximately one-quarter wavelength beyond the point of crossing. With matching techniques, a bandwidth of an octave or so should be feasible.

Fig. 4 shows one way that a wide-band transition between miniature-cross-section coaxial line and slot line can be made. Additional structural details may be needed to obtain optimum matching and to prevent radiation loss.

A half-wavelength slot, as shown in Fig. 5(a), can be used as a resonator. If desired, the resonant slot may be made more compact by capacitively loading its center, as in Fig. 5(b), or by bending it, as in Fig. 5(c). Applications to bandstop and bandpass filters are shown in Fig. 6. In the bandstop example, the terminating lines are microstrip, and in the bandpass example they are slot lines. Many other filter configurations are feasible, using slots alone or slots with strips on the opposite side of the substrate.

The basic electrical parameters of slot line are the characteristic impedance Z_0 and the phase velocity v. Because of the non-TEM nature of the slot-line mode these parameters are not constant, but vary with frequency at a rather slow rate per octave. This behavior contrasts with quasi-TEM

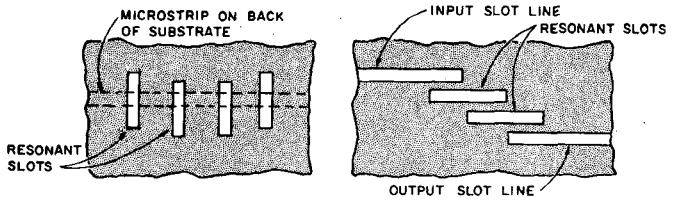

Fig. 6. Filter applications. (a) Bandstop filter. (b) Bandpass filter.

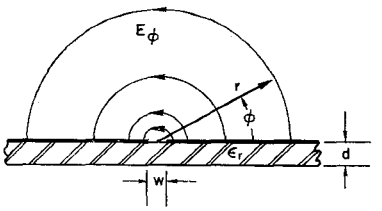

Fig. 7. Cylindrical coordinates with axis on center line of slot.

microstrip line, whose Z_0 and v are first-order independent of frequency. On the other hand, slot line differs from waveguide in that it has no cutoff frequency. Propagation along the slot occurs at all frequencies down to $f=0$, where, if the metal-coated substrate is assumed infinite in length and width, v/c approaches unity and Z_0 approaches zero. Other parameters treated in this paper are the ratio of phase and group velocities v/v_g and the effect of adjacent walls. Attenuation has not yet been treated, but data thus far indicates it to be about the same as for microstrip on the same substrate [20].

II. Approximations for Slot Line

Several references on slot antennas were found in which the presence of a substantial amount of dielectric material in or near the slot was taken into account. Strumwasser, Short, Stegen, and Miller [4] have studied experimentally the effects of filling a slot in a thick metal plate with dielectric material. They give data on resonant-length reduction and radiation resistance coupled into an air-dielectric TEM line. Bailey [5] has measured resonant length and radiation conductance of a slot in a waveguide wall covered by a protective layer of dielectric material. Galejs [6] has analyzed theoretically a slot in a zero-thickness, perfectly conducting sheet separating free space from a lossy dielectric medium of infinite extent. For example, a slot radiator in a wire mesh on the surface of the ground would be simulated by this model.

Galejs utilizes an integral-equation method to obtain complex expressions for radiation efficiency and other parameters of the slot antenna. His *zero-order* solution for the propagation constant along the slot can be easily modified into the following simple formula for relative wavelength:

$$\frac{\lambda'}{\lambda} = \sqrt{\frac{2}{\epsilon_r + 1}}. \tag{1}$$

Since wavelength is inversely proportional to the square root of permittivity, an effective permittivity of a uniform medium replacing the two different dielectric half spaces may be defined as

$$\epsilon_r' = \frac{\epsilon_r + 1}{2}. \tag{2}$$

The *second-order* solution for slot line derived in this paper shows that (1) is a fair approximation for slot line, yielding values within about 10 percent in typical slot-line cases. The second-order solution shows quantitatively how λ'/λ varies with the parameters d, w, ϵ_r, and λ.

The field components on the air side of the slot can be computed quite easily as a function of λ, λ', and distance r from the slot (Fig. 7). If we assume $w/\lambda \ll 1$, then the electric voltage across the slot may be replaced by an equivalent line source of magnetic current. At a distance r at least several times larger than w the longitudinal component of magnetic field is given by [7]

$$H_z = AH_0^{(1)}(k_c r) \tag{3}$$

where $H_n^{(1)}(x)$ is the Hankel function of first kind, order n, and argument x. The coefficient k_c is

$$k_c = \sqrt{\gamma_z^2 + k^2} = j\frac{2\pi}{\lambda}\sqrt{\left(\frac{\lambda}{\lambda'}\right)^2 - 1} \tag{4}$$

since $\gamma_z = j2\pi/\lambda_z = j2\pi/\lambda'$ and $k = 2\pi/\lambda$.

By (1), a zero-order value of k_c is

$$k_c = j\frac{2\pi}{\lambda}\sqrt{\frac{\epsilon_r - 1}{2}}. \tag{5}$$

The other field components are H_r and E_ϕ. They are related to H_z by [7]

$$H_r = -\frac{\gamma_z}{k_c^2}\frac{\partial H_z}{\partial r} = \frac{A}{\sqrt{1 - \left(\frac{\lambda'}{\lambda}\right)^2}} H_1^{(1)}(k_c r) \tag{6}$$

$$E_\phi = \frac{j\omega\mu}{k_c^2}\frac{\partial H_z}{\partial r} = \frac{-\eta(\lambda'/\lambda)A}{\sqrt{1 - \left(\frac{\lambda'}{\lambda}\right)^2}} H_1^{(1)}(k_c r) \tag{7}$$

where the identity $d[H_0^{(1)}(x)]/dx = -H_1^{(1)}(x)$ was used.

The Hankel function of imaginary argument, $H_n^{(1)}(j|x|)$, approaches zero proportional to $e^{-|x|}/\sqrt{|x|}$ for $|x|$ large. Equation (4) shows that the argument $k_c r$ is imaginary for $\lambda'/\lambda < 1$. Hence a relative wavelength ratio less than unity is a sufficient condition to ensure decay of the slot-mode field with radial distance. As λ'/λ is decreased, the decay becomes sharper and the fields become more tightly bound to the slot.

A radius r_{cp} of circular polarization of the magnetic field requires $|H_z/H_r| = 1$. By means of (3) and (6), r_{cp} must satisfy

$$\left|\frac{H_1^{(1)}(k_c r_{cp})}{H_0^{(1)}(k_c r_{cp})}\right| = \sqrt{1 - \left(\frac{\lambda'}{\lambda}\right)^2}. \tag{8}$$

However, tables show that $|H_1^{(1)}(j|x|)| > |H_0^{(1)}(j|x|)|$ for all $|x|$ [8]. Since the right-hand side of (8) is less than one, a solution for r_{cp} does not exist. Nevertheless, elliptical polarization occurs for all r, and low axial ratios occur for r sufficiently large.

Also of interest is the ratio of voltage along a semicircular path at constant radius divided by the voltage directly across the slot. This ratio is

$$\frac{V(r)}{V} = \frac{k_c r H_1^{(1)}(k_c r)}{\lim_{|x|\to 0} [\,|x| H_1^{(1)}(j|x|)]} = \frac{\pi}{2} k_c r \left| H_1^{(1)}(k_c r) \right| . \tag{9}$$

As an example of field decay, let $\epsilon_r = 16$, $f = 3$ GHz, and $\lambda = 4$ inches. The zero-order value of λ'/λ is 0.343, and of $k_c r$ is 4.30 r, where r is in inches. At $r = 0$, 0.7, 1.0, and 1.3 inches, $V(r)/V = 1$, 0.120, 0.0382, and 0.0118, respectively. If a plane metal wall is positioned perpendicular to the radius vector at distance $r/2$ from the slot, an image of the slot will appear at distance $r/2$ behind the wall. The effect will be that of two equally excited parallel slots spaced by r. Thus if the metal wall is at distance 0.5 inch in the above example, $r = 1$ inch and $V(r)/V$ of one slot is 0.0382, or -28.36 dB, at the other slot. Coupling between slots is even weaker than this, since only part of the total voltage $V(r)$ of one slot affects the other slot. Therefore, a wall or other perturbing object can be as close as $r = 0.5$ inch with little effect on λ' or Z_0, and the fields and stored energy of the slot mode are mainly confined within this same radial distance. These conclusions have been verified both by experiment and by computations using the second-order solution.

III. Basis of Second-Order Solution

An analytical approach for slot line offering high accuracy is described in this section. The solution obtained by this approach will be referred to as *second-order*. A first-order solution offering intermediate complexity and accuracy between zero-order (1) and second-order equations would also be useful, but has not yet been completed.

The key feature of the approach used in the second-order solution is the introduction of boundary walls permitting the slot-line configuration to be treated as a rectangular-waveguide problem rather than as a problem in cylindrical coordinates. Thus the infinite orthogonal sets of relatively simple rectangular-waveguide modes apply rather than sets of cylindrical modes embodying all orders of Hankel functions.

Parameters evaluated in this paper are: relative-wavelength ratio λ'/λ, characteristic impedance Z_0, ratio of phase velocity to group velocity v/v_0, and the effect of nearby electric and magnetic walls.

Future plans are to adapt the second-order solution to yield the even- and odd-mode characteristic impedances and velocities of parallel slots, the effect of metal-coating thickness greater than zero, attenuation per unit length, unloaded

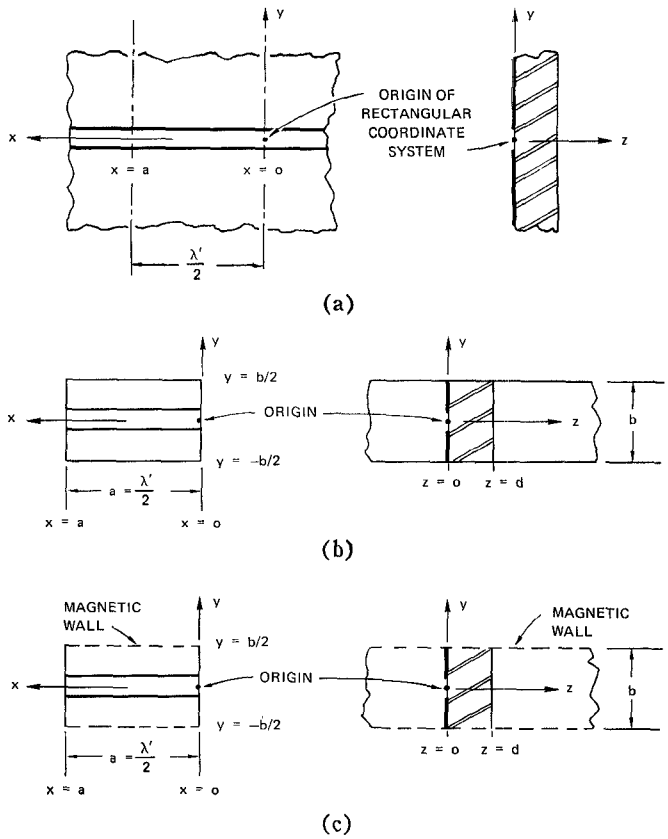

Fig. 8. Development of waveguide models for slot-line solution. (a) Insertion of transverse conducting planes at $x = 0$ and a. (b) Insertion of conducting planes at $y = \pm b/2$. (c) Insertion of magnetic walls at $y = \pm b/2$.

Q of a resonant slot, and presence of more than one dielectric substrate on one or both sides of the slotted conductive sheet.

Conversion of the slot-line configuration into a rectangular-waveguide problem is illustrated in Fig. 8. First assume that slot waves of equal amplitude are traveling in the $+x$ and $-x$ directions. Then transverse planes spaced by $\lambda'/2$ exist where the transverse E field and normal H field cancel to zero. Let two such planes occur at $x = 0$ and $x = \lambda'/2 = a$ in Fig. 8(a). Conducting (or electric) walls of infinite extent may be inserted in these planes without disturbing the field components between the planes, and the semi-infinite regions at $x < 0$ and $x > a$ may be eliminated. The section of slot line between the transverse planes supports a resonant slot-wave mode with no loss of energy, if the dielectric substrate and the conducting walls are assumed dissipationless.

Next, conducting walls are inserted in planes parallel to the slot and perpendicular to the substrate at $y = \pm b/2$. The region separated out of the original infinite space has the rectangular-waveguide boundary shown in Fig. 8(b). Since the fields are tightly bound to the vicinity of the slot, the walls at $y = \pm b/2$ will have negligible effect for b sufficiently large (typically one inch at 3 GHz), yet they serve the important function of enabling the use of rectangular-waveguide mode sets, thereby greatly simplifying the analysis.

Magnetic walls may be placed at $y \doteq \pm b/2$ instead of electric walls. The result is the boundary shown in Fig. 8(c),

where two magnetic walls spaced by b and two electric walls spaced by a are used.

Images of the slot in the electric or magnetic walls at $y=\pm b/2$ result in an infinite array of parallel slots in the $z=0$ plane having center-to-center spacing of b. Therefore, the effect of adjacent slots may be computed for both electric- and magnetic-wall imaging, allowing the even- and odd-mode characteristic impedances and wavelengths to be evaluated for a slot in an infinite array. For one pair of slots rather than an array, these even- and odd-mode quantities are given approximately by the $b\to\infty$ values modified by one half the change computed for the infinite array.

Thus, the introduction of walls in Fig. 8 has created the configuration of a capacitive iris in a rectangular waveguide, with air and dielectric regions as indicated. Consider the metal-walled case in Fig. 8(b). All waveguide modes must have the $\lambda'/2$ variation of the slot wave in the x direction. Also, because of the symmetry of the structure, all modes must have an E-field maximum at the center of the slot. Therefore, the full set of modes satisfying the boundary conditions are TE_{10}, TE_{12}, TE_{14}, $\cdots$, and TM_{12}, TM_{14}, $\cdots$; that is, $TE_{1,2n}$ for n an integer ≥ 0 and $TM_{1,2n}$ for $n\geq 1$.

For the slot wave, $\lambda'<\lambda$ and hence $a<\lambda/2$. Therefore, the TE_{10} and all higher modes are cut off, or nonpropagating, in the air regions. In the dielectric region the TE_{10} mode is propagating, and the first few higher modes may propagate or all higher modes may be cut off, depending on the size of b. Since all modes are cut off in the two air regions, the energy of the resonant slot-wave mode is trapped near the slot. The amplitude of each mode in each region must be such that when the full set of modes are superimposed, the boundary conditions in the iris plane at $z=0$ will be met, and all field components on either side of the dielectric-to-air interface at $z=d$ will be matched. An alternative but equivalent condition is that transverse resonance occur; that is, the sum of the susceptances at the iris plane must equal zero. This sum includes the susceptances of the TE_{10} mode looking in the $-z$ and $+z$ directions, and the capacitive-iris susceptance representing higher modes on the $-z$ and $+z$ sides of the iris.

A formula for characteristic impedance is derived in Appendix II by a method utilizing the total-susceptance formula. Because of the non-TEM nature of the slot wave, definition of characteristic impedance is somewhat arbitrary. The reasonable and useful definition chosen here is $Z_0=V^2/2P$, where $V=-\int E_y dy$ is peak voltage amplitude across the slot and P is average power flow of the wave. As in waveguide, this definition does not necessarily yield the best match in a transition to coaxial or microstrip line. In fact, experimental results indicate that a 50 ohm coaxial or microstrip line requires about 75 ohm slot impedance computed by the voltage power definition [19], [20]. Reactive discontinuity effects may also play a part in this discrepancy.

IV. Parameter Formulas—Second-Order Solution

Define as an independent variable $p=\lambda/2a$. At the transverse-resonance frequency, $a=\lambda'/2$ and hence $p=\lambda/\lambda'$ for $B_t=0$ where B_t is the total susceptance at the plane of the slot. Once $p=\lambda/\lambda'$ has been determined as the solution of $B_t=0$ for a given set of parameters ϵ_r, w, d, b, and a, the wavelength and frequency for this solution are simply $\lambda=2a(\lambda/\lambda')$ and $f=c/\lambda$.

The formula for B_t is as follows for the case of electric walls at $y=\pm b/2$:

$$\eta B_t=\frac{a}{2b}\left[-v+u\tan\left(\frac{\pi du}{ap}-\tan^{-1}\frac{v}{u}\right)\right]+\frac{1}{p}\left\{\left(\frac{\epsilon_r+1}{2}-p^2\right)\ln\frac{2}{\pi\delta}+\frac{1}{2}\cdot\sum_{n=1,2,3,\cdots}\left[v^2\left(1-\frac{1}{F_n}\right)+M_n\right]\frac{\sin^2(\pi n\delta)}{n(\pi n\delta)^2}\right\}, \tag{10}$$

and as follows for magnetic walls at $y=\pm b/2$:

$$\eta B_t=\frac{1}{p}\left\{\left(\frac{\epsilon_r+1}{2}-p^2\right)\ln\frac{8}{\pi\delta}+\frac{1}{2}\cdot\sum_{n=\frac{1}{2},\frac{3}{2},\frac{5}{2},\cdots}\left[v^2\left(1-\frac{1}{F_n}\right)+M_n\right]\frac{\sin^2(\pi n\delta)}{n(\pi n\delta)^2}\right\} \tag{11}$$

where $\eta=\sqrt{\mu_0/\epsilon_0}=376.7$ ohms, $\delta=w/b$, and

$$u=\sqrt{\epsilon_r-p^2},\qquad v=\sqrt{p^2-1} \tag{12}$$

$$F_n=\sqrt{1+\left(\frac{b}{2an}\cdot\frac{v}{p}\right)^2},$$

$$F_{n1}=\sqrt{1-\left(\frac{b}{2an}\cdot\frac{u}{p}\right)^2}. \tag{13}$$

For F_{n1} real, M_n is

$$M_n=\frac{\epsilon_r\tanh r_n-p^2F_{n1}^2\coth q_n}{\left[1+\left(\frac{b}{2an}\right)^2\right]F_{n1}}-u^2 \tag{14}$$

where

$$r_n=\frac{2\pi ndF_{n1}}{b}+\tanh^{-1}\left(\frac{F_{n1}}{\epsilon_rF_n}\right) \tag{15}$$

$$q_n=\frac{2\pi ndF_{n1}}{b}+\coth^{-1}\left(\frac{F_n}{F_{n1}}\right). \tag{16}$$

For F_{n1} imaginary, M_n is

$$M_n=\frac{\epsilon_r\tan r_n'-p^2|F_{n1}|^2\cot q_n'}{\left[1+\left(\frac{b}{2an}\right)^2\right]|F_{n1}|}-u^2 \tag{17}$$

where

$$r_n'=\frac{2\pi nd|F_{n1}|}{b}+\tan^{-1}\left(\frac{|F_{n1}|}{\epsilon_rF_n}\right) \tag{18}$$

$$q_n'=\frac{2\pi nd|F_{n1}|}{b}+\cot^{-1}\left(\frac{F_n}{|F_{n1}|}\right). \tag{19}$$

Equations (10) and (11) for B_t are valid for $\delta = w/b \leq 0.15$, $w < \lambda/(4\sqrt{\epsilon_r})$, and $w \leq d$. These ranges are more than adequate for usual slot-line dimensions.

The procedure in using the above equations is to substitute a set of values ϵ_r, w, d, b, and $a = \lambda'/2$, and then to solve (10) or (11) for the value of p at which $\eta B_t = 0$. This p is equal to λ/λ'. Wavelength and frequency are then given by $\lambda = 2a(\lambda/\lambda')$ and $f = c/\lambda$. Solution of the above equations is most conveniently accomplished with an electronic computer, arriving at $B_t = 0$ by an iterative process.

The group velocity is $v_g = d\omega/d\beta$, where $\omega = 2\pi f$ and β is the slot-wave phase constant in radians per unit length. From this definition of v_g, one may obtain the following relations for the ratio of phase velocity to group velocity:

$$\frac{v}{v_g} = 1 + \frac{f}{\lambda'/\lambda} \cdot \frac{-\Delta(\lambda'/\lambda)}{\Delta f} = 1 + \frac{f}{\lambda/\lambda'} \cdot \frac{\Delta(\lambda/\lambda')}{\Delta f} \tag{20}$$

where $\Delta(\lambda'/\lambda)$, $\Delta(\lambda/\lambda')$, and Δf are computed from two separate solutions of $\eta B_t = 0$ for fixed values of ϵ_r, w, d, and b, and for two slightly different values of $a = \lambda'/2$ incremented plus and minus from the desired a. The frequency f may be assumed to lie midway in the Δf interval.

The slot-wave characteristic impedance is obtained as follows from the ηB_t formulas:

$$Z_0 = 376.7 \frac{v}{v_g} \frac{\pi}{p} \cdot \frac{\Delta p}{-\Delta \eta B_t} \text{ ohms.} \tag{21}$$

In this equation $\Delta \eta B_t$ is computed from (10) or (11) with ϵ_r, w, d, b, and a held constant, and with p incremented slightly plus and minus from the value $p = \lambda/\lambda'$ at $\eta B_t = 0$; v/v_g is obtained from (20) for the same parameters. Equations (20) and (21) may be used with (10) to yield values for electric walls at $y = \pm b/2$, or with (11) for magnetic walls.

V. Computed Data

The second-order solution equations in Section IV were programmed on an electronic computer and the parameters λ'/λ, v/v_g, and Z_0 were computed for various slot-line cases.[1]

Fig. 9 shows the effect of wall spacing b on the parameters for both electric and magnetic walls. In this computation, $\epsilon_r = 20$, $d = 0.137$ inch, $w = 0.025$ inch, and λ' is constant at 1.360 inches. The corresponding curves for electric and magnetic walls merge together for $b > 1.5$ inches and are only slightly separated for $b = 1$ inch. As b decreases below 1 inch, the λ'/λ curves diverge more and more rapidly. Since λ' is held constant, λ varies inversely and f proportionally with λ'/λ. The ratio v/v_g decreases with b for magnetic walls and increases for electric walls. The behavior of the characteristic impedance is more complex, the electric-wall curve rising and then falling sharply as b decreases, and the magnetic-wall curve falling and then rising sharply. This reversal of direction is caused by the v/v_g factor in (21). The quantity $Z_0/(v/v_g)$ is virtually constant for the two types of walls for

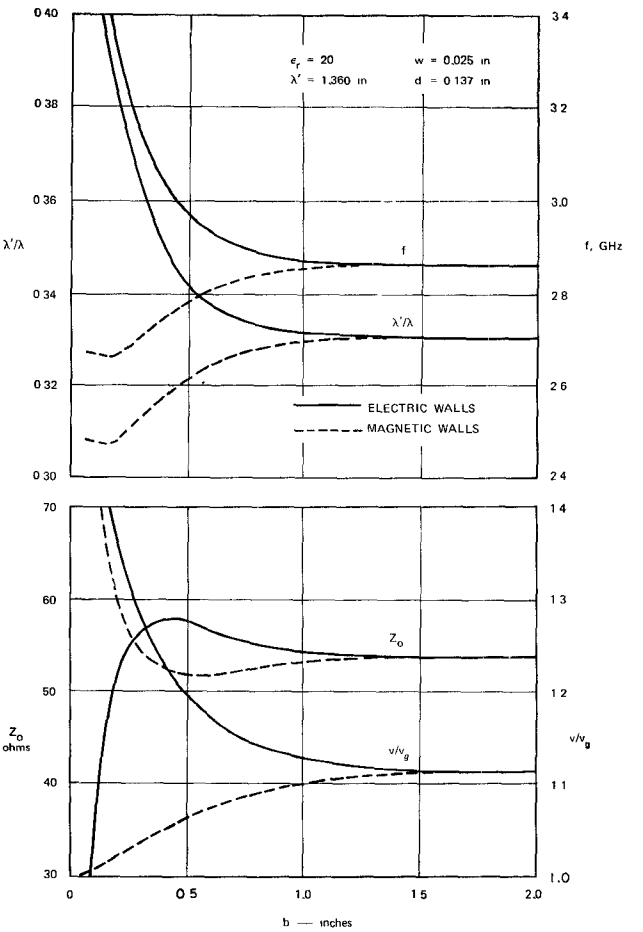

Fig. 9. Slot-line parameters versus b with ϵ_r, w, d and $a = \lambda'/2$ fixed.

b as low as 0.6 inch, while for b smaller, this quantity diverges without changing direction.

The variation of Z_0 and λ'/λ with frequency is shown in Fig. 10 for $\epsilon_r = 20$, $d = 0.137$ inch, $w = 0.025$ inch, and for $\lambda' = 2a$ stepped from 0.5 to 150 inches in the computation. Curves are plotted for $b = 3$ inches and $b \to \infty$ (that is, b sufficiently large at each λ' value such that Z_0 and λ'/λ are essentially independent of b). The ratio λ'/λ decreases monotonically in the plotted range. For increasing f, λ'/λ falls toward $1/\sqrt{\epsilon_r} = 0.224$, while for f approaching zero λ'/λ rises to 0.390 for magnetic walls at $b = 3$ inches and to 1.0 for the two other curves. The zero-order value of λ'/λ calculated from (1) is indicated for comparison.

The characteristic impedance plotted in Fig. 10 has a broad maximum, varying by only ± 7 percent between 1 and 6 GHz. As f approaches zero, Z_0 approaches 40.3 ohms for magnetic walls at $b = 3$ inches, and approaches 0 ohms for the other two cases.

A few experimental λ'/λ points are shown in Fig. 10. The substrate used in the test piece had a specified ϵ_r of 20. Length, width, and thickness were approximately 5 by 1.75 by 0.137 inches. For the circled points one side was covered with Scotch Brand No. 51 aluminum tape, about 0.0007 inch thick, including 0.0001 inch of adhesive. A slot 0.025 inch wide and 3 inches long was left bare. A probe terminating a

[1] Normalized graphs of λ'/λ and Z_0 versus d/λ for $w/d = 0.02$, 0.1, 0.2, 0.4, and 0.6, and for $\epsilon_r = 13$, 16, and 20 have been prepared and are included in another paper [19].

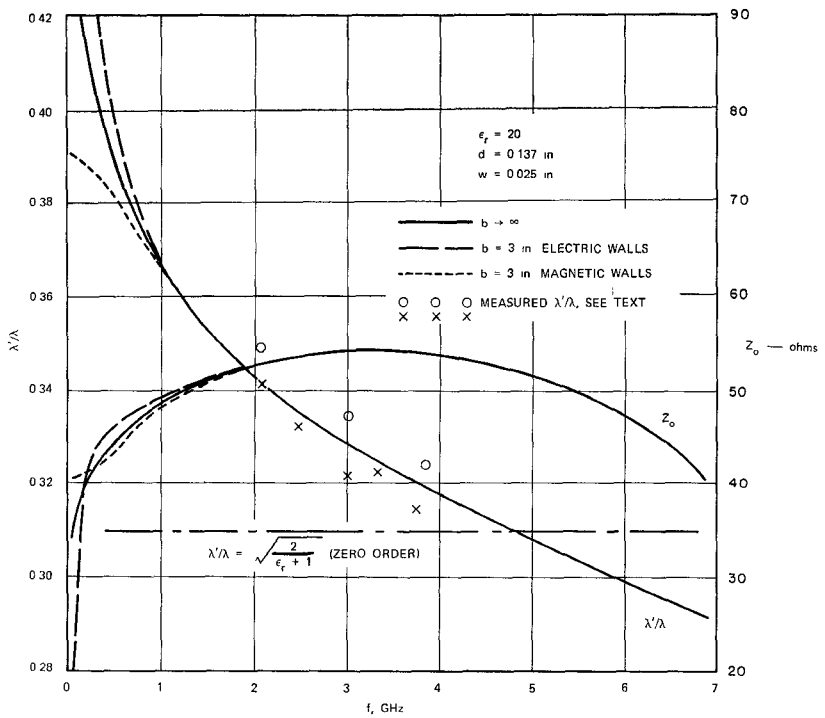

Fig. 10. Graph of λ'/λ and Z_0 versus frequency.

reflectometer coupler was coupled to the slot near one end. Resonance was indicated by a dip in the reflected wave. The slot length was varied by sliding a thin steel scale over the slot from the end opposite the probe. At each of the test frequencies the overlapping length of steel scale was varied until resonance was found. Several lengths for resonance were obtained differing in $\lambda'/2$ steps, thus yielding λ' and λ'/λ. The circled points lie parallel to the theoretical λ'/λ curve, but about 2.3 percent above it. For the crossed points, the same substrate sample was tested with copper plating directly applied. The thickness was about 0.0008 inch and slot width was 0.0235 inch. These points lie about 1.1 percent below the theoretical curve. The difference between the two sets of points may be attributed to the thin layer of adhesive on the aluminum tape. Additional tests with other permittivities and other w, d, and λ yield similar agreement with λ'/λ computations [19].

The effect of varying slot width w on λ'/λ and Z_0 is shown in Fig. 11 for two different cases of ϵ_r and d. In each case λ' is held constant. The ratio λ'/λ increases with w, but only slightly. The characteristic impedance Z_0 increases substantially, although far less than in proportion to w.

Measurements of Z_0 have not yet been made.[2] However, the computed Z_0 values for the magnetic-wall case can be checked when $b/\lambda' \ll 1$, since in the static limit this slot-line cross section becomes equivalent to a TEM-mode transmis-

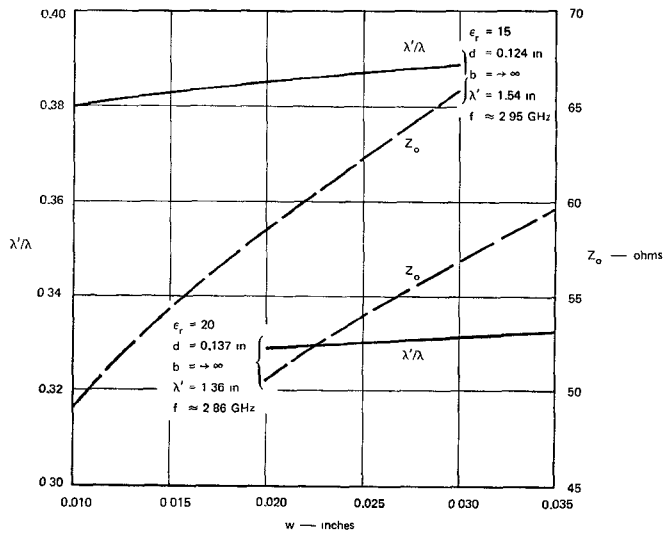

Fig. 11. Graph of λ'/λ and Z_0 versus slot width.

sion line containing an equivalent dielectric medium $\epsilon_r' = (\lambda/\lambda')^2$. The Z_0 formula for this TEM line may be obtained by a straightforward modification of a case treated in [18]:

$$Z_0 = \frac{591.7}{\sqrt{\epsilon_r'}\ln\left(\frac{8b}{\pi w}\right)} = \frac{591.7(\lambda'/\lambda)}{\ln\left(\frac{8b}{\pi w}\right)} \text{ ohms} \qquad \begin{matrix} b/w > 3 \\ b/\lambda' \to 0. \end{matrix} \tag{22}$$

[2] Good transitions have been achieved at C and X bands between slot line and 50 ohm coaxial and microstrip lines with $\epsilon_r = 16$, $d = 0.055$ inch, and $w = 0.021$ inch [20]. Another good transition at S band had $\epsilon_r = 16$, $w = 0.031$ inch, and $d = 0.062$ inch [19]. See the discussion at the end of Section III on the arbitrary nature of slot-line Z_0 definition.

TABLE I
COMPARISON OF SECOND-ORDER AND STATIC SOLUTIONS FOR Z_0

Second-Order Solution			Eq (22)
b (inches)	λ'/λ	Z_0 (Ω)	Z_0 (Ω)
0.10	0.30752	78.38	78.40
0.14	0.30707	68.35	68.37
0.20	0.30763	60.45	60.39
0.30	0.31230	54.60	54.04
0.40	0.31640	52.42	50.50
0.60	0.32384	51.77	46.59

In Table I, (22) is tested against data computed for the curves of Fig. 9 ($\epsilon_r=20$, $d=0.137$ inch, $w=0.025$ inch, $\lambda'=1.360$ inches, $f\approx 2.670$ GHz). Agreement is excellent for $b\leq 0.20$ inch or $b/\lambda'\leq 0.15$. A second test is afforded by a computed point used in plotting the graph in Fig. 10. For $\epsilon_r=20$, $d=0.137$ inch, $w=0.025$ inch, $b=3.00$ inches, and $\lambda'=150.0$ inches, the second-order solution gives $\lambda'/\lambda=0.38987$, $f=30.67$ MHz, and $Z_0=40.33$ ohms. Equation (22) yields 40.32 ohms.

APPENDIX I
DERIVATION OF B_t FORMULAS

Fig. 12 shows a longitudinal yz-plane view through the waveguide model for the slot-line analysis. The waveguide boundaries in this case are conducting, or electric, walls. The TE_{10}-mode susceptance at the iris plane ($z=0$) is B_d looking to the right into the dielectric slab and B_a looking to the left into the air region. The total susceptance in the iris plane is $B_t=B_d+B_a$.

A formula for B_d will be derived first and then modified to yield B_a. The approach is based on a previously published analysis of a waveguide filter consisting of an alternating series of steps between two cross-section heights [9], [10], and on earlier analyses applied to other discontinuities [11], [12]. Fig. 13 shows the basic structure treated in [9] and [10], with notation modified for slot line. A waveguide of height b is driven by a waveguide of height w, with an abrupt step at $z=0$. A reactive plane is placed transverse to the waveguide at $z=l$. This terminating plane can be either an electric or magnetic wall.

Since all walls and the dielectric material are assumed lossless, the admittance looking to the right at $z=0$ is a pure susceptance, B_d. Because of symmetry, only $TE_{1,2n}$ (with $n\geq 0$) and $TM_{1,2n}$ (with $n\geq 1$) modes are present. In a transverse plane the E_y and H_x components of each mode are proportional to $\sin \pi x/a \cos 2\pi ny/b$. Thus the total E_y and H_x fields at the $z=0$ plane and $x=a/2$ are functions of y as follows:

$$E_y = R_0 + \sum_{n>0} R_n \cos\frac{2\pi ny}{b} \tag{23}$$

$$H_x = -y_{i0}R_0 - \sum_{n>0} y_{in}R_n \cos\frac{2\pi ny}{b} \tag{24}$$

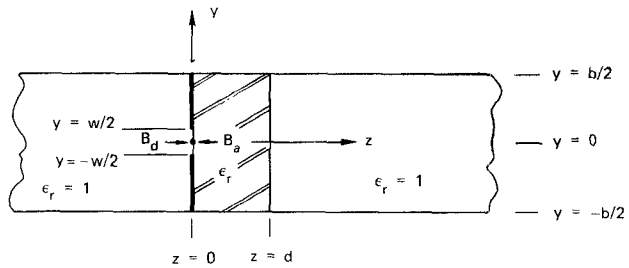

Fig. 12. Waveguide model containing capacitive iris and dielectric slab.

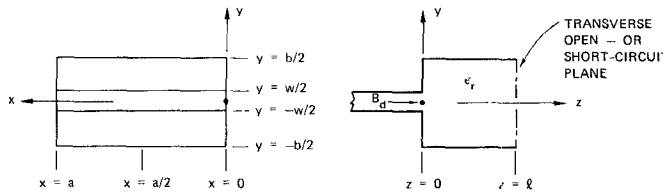

Fig. 13. Waveguide of height b driven by waveguide of height w.

where $n=1, 2, 3, \cdots$, R_0 and R_n are constants, and input wave admittances y_{i0} and y_{in} are defined by

$$y_{i0} = -\left(\frac{H_x}{E_y}\right)_{TE_{10}} \tag{25}$$

$$y_{in} = -\left(\frac{(H_x)_{TE_{1,2n}} + (H_x)_{TM_{1,2n}}}{(E_y)_{TE_{1,2n}} + (E_y)_{TM_{1,2n}}}\right). \tag{26}$$

The analysis will be simplified by assuming that only the TE_{10} mode is present in the waveguide of height w at $z=0$. Therefore, E_y and H_x are constants as follows:

$$E_y = \begin{cases} C_0 & \text{for } |y| \leq w/2 \\ 0 & \text{for } w/2 < |y| \leq b/2 \end{cases} \tag{27}$$

$$H_x = -C_0 y_i' \quad \text{for } |y| \leq w/2 \tag{28}$$

where y_i' is input wave admittance in the waveguide of height w at the plane $z=0$. The error in the analysis due to neglecting higher modes in the region $z<0$ is very small for $\delta=w/b$ small, as would be usual for slot line.

Equation (23) has the form of a Fourier series. Let this series equal E_y as defined by (27). Then R_0 and R_n are determined as follows:

$$R_0 = C_0\delta, \qquad R_n = 2C_0\delta\frac{\sin \pi n\delta}{\pi n\delta}. \tag{29}$$

Next, set the right-hand sides of (24) and (28) equal, and integrate with respect to y over the opening of height w to obtain

$$C_0 y_i' = y_{i0}R_0 + \sum_{n>0} y_{in}R_n \frac{\sin \pi n\delta}{\pi n\delta} \tag{30}$$

and, by (29),

$$(b/w)y_i' = y_{i0} + 2\sum_{n>0} y_{in}\left(\frac{\sin \pi n\delta}{\pi n\delta}\right)^2. \tag{31}$$

At this point replace the wave admittances by guide admittances defined on the TE_{10}-mode voltage power basis in the complete waveguide cross section [13]; that is, replace y_{in} by $Y_{in}=(a/2b)y_{in}$ and y_i' by $Y_i=(a/2w)y_i'$. Then

$$Y_i = jB_d = Y_{i0} + 2\sum_{n>0} Y_{in}\left(\frac{\sin \pi n\delta}{\pi n\delta}\right)^2. \tag{32}$$

With reference to Fig. 12, Y_{i0} is the admittance seen by a TE_{10} wave directed into a dielectric-filled waveguide region of length d terminated by an infinite air-filled region:

$$Y_{i0} = jY_{o1}\tan\left(\beta_1 d + \tan^{-1}\frac{Y_0}{jY_{o1}}\right). \tag{33}$$

In the notation used in (33), symbols with the subscript 1 apply to the dielectric-filled region between $z=0$ and $z=d$; without this subscript they apply to the air regions. Y_{o1} and Y_o are TE_{10}-mode characteristic admittances and $\beta_1=\gamma_1/j=2\pi/\lambda_{g1}$ is the TE_{10}-mode phase constant.

$$Y_0 = \frac{a\gamma}{j2b\eta k}, \quad Y_{o1} = -j\frac{a\gamma_1}{2b\eta_1 k_1} = \frac{a}{2b\eta}\cdot\frac{\lambda}{\lambda_{g1}} \tag{34}$$

where $\eta=\sqrt{\mu_0/\epsilon_0}=376.7$ ohms and $\eta_1=\eta/\sqrt{\epsilon_r}$; γ and γ_1 are the TE_{10}-mode z-directed propagation constants; $k=2\pi/\lambda$ and $k_1=2\pi\sqrt{\epsilon_r}/\lambda$ are the plane-wave constants; and λ_{g1} is the TE_{10}-mode guide wavelength in the ϵ_r region.

For $n>0$, both $TE_{1,2n}$ and $TM_{1,2n}$ modes are present. For each n, the corresponding TE and TM amplitudes must be chosen so that E_x exactly cancels at $z=0$. In this way the total E_x field will be zero at $z=0$, as is required by the boundary conditions in that transverse plane. From (26) we obtain for the nth mode

$$Y_{in} = \frac{Y_{iTMn} + Y_{iTEn}D_n}{1 + D_n} \tag{35}$$

where

$$D_n = \frac{(E_y)_{TE1,2n}}{(E_y)_{TM1,2n}} \text{ when } (E_x)_{TE1,2n} + (E_x)_{TM1,2n} = 0. \tag{36}$$

From the field-component formulas for the TE and TM modes [7], [9] we obtain

$$D_n = \left(\frac{b}{2an}\right)^2. \tag{37}$$

The input admittances Y_{iTMn} and Y_{iTEn} for each n are[3]

$$Y_{iTMn} = Y_{o1TMn}\tanh\left(\gamma_{n1}d + \tanh^{-1}\frac{Y_{oTMn}}{Y_{o1TMn}}\right) \tag{38}$$

$$Y_{iTEn} = Y_{o1TEn}\coth\left(\gamma_{n1}d + \coth^{-1}\frac{Y_{oTEn}}{Y_{o1TEn}}\right) \tag{39}$$

where the characteristic admittances and propagation constants are

$$Y_{o1TMn} = \frac{jak_1}{2b\eta_1\gamma_{n1}}, \quad Y_{oTMn} = \frac{jak}{2b\eta\gamma_n} \tag{40}$$

$$Y_{o1TEn} = \frac{a\gamma_{n1}}{j2b\eta_1 k_1}, \quad Y_{oTEn} = \frac{a\gamma_n}{j2b\eta k} \tag{41}$$

$$\gamma_{n1} = \sqrt{\left(\frac{2\pi n}{b}\right)^2 + \left(\frac{\pi}{a}\right)^2 - \left(\frac{2\pi}{\lambda}\right)^2\epsilon_r} = \frac{2\pi n}{b}\sqrt{1 - \left(\frac{b}{n\lambda_{g1}}\right)^2} \tag{42}$$

$$\gamma_n = \frac{2\pi n}{b}\sqrt{1 + \left(\frac{b\gamma}{2\pi n}\right)^2}. \tag{43}$$

Then (35) and (37) through (41) yield

$$\eta Y_{in} = j\frac{ak}{2b\gamma_{n1}}\cdot\frac{\epsilon_r\tanh r_n - \left(\frac{b\gamma_{n1}}{2ank}\right)^2\coth q_n}{1 + \left(\frac{b}{2an}\right)^2} \tag{44}$$

$$r_n = \gamma_{n1}d + \tanh^{-1}\left(\frac{\gamma_{n1}}{\epsilon_r\gamma_n}\right) \tag{45}$$

$$q_n = \gamma_{n1}d + \coth^{-1}\left(\frac{\gamma_n}{\gamma_{n1}}\right). \tag{46}$$

Now let $p=\lambda/2a$ and

$$u = \frac{\lambda}{\lambda_{g1}} = \frac{\gamma_1}{jk} = \sqrt{\epsilon_r - p^2} \tag{47}$$

$$v = \frac{\gamma}{k} = \sqrt{p^2 - 1} \tag{48}$$

$$F_{n1} = \frac{b\gamma_{n1}}{2\pi n} = \sqrt{1 - \left(\frac{b}{n\lambda_{g1}}\right)^2} = \sqrt{1 - \left(\frac{bu}{2anp}\right)^2} \tag{49}$$

$$F_n = \frac{b\gamma_n}{2\pi n} = \sqrt{1 + \left(\frac{bv}{2anp}\right)^2}. \tag{50}$$

Equations (32) through (34) and (44) through (50) yield

$$\eta B_d = \frac{au}{2b}\tan\left(\frac{\pi ud}{ap} - \tan^{-1}\frac{v}{u}\right) + \frac{1}{2p} \cdot \sum_{n=1,2,\cdots}\left[\frac{\epsilon_r\tanh r_n - p^2F_{n1}^2\coth q_n}{\left[1 + \left(\frac{b}{2an}\right)^2\right]F_{n1}}\right]\cdot\frac{\sin^2\pi n\delta}{n(\pi n\delta)^2}. \tag{51}$$

The first term is the TE_{10}-mode susceptance; the second term is the discontinuity susceptance representing the effect of higher modes. The rate of convergence of the series is very slow but will be improved by the following procedure. If we let $d\to\infty$ and $f\to 0$, then $\lambda'=2a\to\infty$ and each term S_n of the series becomes

$$S_n' = \frac{u^2\sin^2\pi n\delta}{n(\pi n\delta)^2}. \tag{52}$$

[3] In (38) and (39), the pair of functions tanh and $\tanh^{-1}$ is interchangeable with coth and $\coth^{-1}$. The selection here is appropriate since $Y_{oTMn}/Y_{o1TMn}<1$ and $Y_{oTEn}/Y_{o1TEn}\geq 1$.

The original series may be replaced by

$$\sum_{n=1,2,\cdots} S_n = \sum_{n=1,2,\cdots} (S_n - S_n') + \sum_{n=1,2,\cdots} S_n'. \quad (53)$$

The first series on the right of the equal sign converges rapidly compared to the series in (51), while the second may be summed in closed form by the following identity [11], [15]:

$$\lim_{\delta\to 0} \sum_{n=1,2,3,\cdots} \frac{\sin^2 \pi n\delta}{n(\pi n\delta)^2} = \ln \frac{1}{2\pi\delta} + \frac{3}{2} = \ln \frac{1}{\delta} - 0.3379. \quad (54)$$

The accuracy of this is excellent for $\delta \leq 0.15$. At $\delta = 0.15$ the error is only 0.4 percent. Therefore, the susceptance of both sides of a capacitive iris is approximately

$$\eta B_C \approx \frac{u^2}{p}\left(\ln \frac{1}{\delta} - 0.3379\right). \quad (55)$$

However, the exact formula in the limit $\lambda_{g1} \to \infty$ is [14]

$$B_C = \frac{4bY_{o1}}{\lambda_{g1}} \ln \csc \frac{\pi\delta}{2} = \frac{u^2}{p} \ln \csc \frac{\pi\delta}{2}, \quad \delta \leq 1$$
$$\approx \frac{u^2}{p} \ln \frac{2}{\pi\delta} = \frac{u^2}{p}\left(\ln \frac{1}{\delta} - 0.452\right), \quad \delta \ll 1. \quad (56)$$

The small difference between the constants in (55) and (56) is the result of assuming in the analysis that E_y and H_x are constant across the slot instead of being the correct functions of y. At this point (53) may be written

$$\sum_{n=1,2,\cdots} S_n = \sum_{n=1,2,\cdots} (S_n - S_n') + u^2 \ln \frac{2}{\pi\delta} \quad (57)$$

where (56) is used instead of (55) for better accuracy. Equation (51) for the susceptance looking into the dielectric section is now

$$\eta B_d = \frac{au}{2b} \tan\left(\frac{\pi ud}{ap} - \tan^{-1}\frac{v}{u}\right) + \frac{u^2}{2p} \ln \frac{2}{\pi\delta} + \frac{1}{2p} \cdot \sum_{n=1,2,\cdots} \left[\frac{\epsilon_r \tanh r_n - p^2 F_{n1}^2 \coth q_n}{\left[1 + \left(\frac{b}{2an}\right)^2\right] F_{n1}} - u^2\right] \frac{\sin^2 \pi n\delta}{n(\pi n\delta)^2}. \quad (58)$$

The susceptance B_a looking toward the left from the iris in Fig. 12 may be obtained from (58) by letting $\epsilon_r = 1$ or $d = 0$. With either substitution, the following equation results:

$$\eta B_a = -\frac{av}{2b} - \frac{v^2}{2p} \ln \frac{2}{\pi\delta} + \frac{1}{2p} \sum_{n=1,2,\cdots} v^2\left(1 - \frac{1}{F_n}\right) \frac{\sin^2 \pi n\delta}{n(\pi n\delta)^2}. \quad (59)$$

When (58) and (59) are added, the total susceptance B_t given by (10) is obtained for electric walls at $y = \pm b/2$.

The susceptance B_t for the case of magnetic walls at $y = \pm b/2$ may be obtained easily from the electric-wall solution. Let the cross section be as shown in Fig. 8(c). Modes excited in the waveguide are TE_{11}, TE_{13}, TE_{15}, $\cdots$ and TM_{11}, TM_{13}, TM_{15}, $\cdots$; that is, $TE_{1,2n}$ and $TM_{1,2n}$ where $n = \frac{1}{2}, \frac{3}{2}, \frac{5}{2}$, etc. The TE_{10} mode cannot exist within this boundary. Careful examination of each step of the above analysis for electric walls shows that (51) applies when the first term representing the TE_{10} contribution is dropped, and when the summation is performed for $n = \frac{1}{2}, \frac{3}{2}, \frac{5}{2}, \cdots$ rather than $n = 1, 2, 3, \cdots$. Evaluation of (54) with $n = \frac{1}{2}, \frac{3}{2}, \frac{5}{2}, \cdots$, yields [15]

$$\lim_{\delta\to 0} \sum_{n=\frac{1}{2},\frac{3}{2},\cdots} \frac{\sin^2 \pi n\delta}{n(\pi n\delta)^2} = \ln \frac{4}{\delta} - 0.3379. \quad (60)$$

Therefore, in (58) for ηB_d and (59) for ηB_a drop the first term, replace $\ln 2/\pi\delta$ by $\ln 8/\pi\delta$, and change the summation index from $n = 1, 2, 3, \cdots$ to $n = \frac{1}{2}, \frac{3}{2}, \frac{5}{2}, \cdots$. The resulting expression giving ηB_t for magnetic walls at $y = \pm b/2$ is (11).

Appendix II

Derivation of Formulas for Z_0 and v/v_g

Define the slot-line characteristic impedance Z_0 by

$$Z_0 = \frac{V_+^2}{2P_+} \quad (61)$$

where P_+ is the average power flow of a slot wave traveling in the $+x$ direction (Fig. 8) and V_+ is the peak amplitude of the voltage across the slot. Now assume a resonant length $\lambda'/2$ of slot line having waves of equal power P^+ and P^- traveling in the $+x$ and $-x$ directions. The total stored energy in this length is $W_t = (P^+ + P^-)(\lambda'/2v_g) = P^+\lambda'/v_g = (2\pi P^+/\omega')(v/v_g)$, where v_g is group velocity, or velocity of energy transport along the slot line [16]. Let V_0 be the maximum voltage at the center of the resonant length of slot. Since the waves in the $+x$ and $-x$ directions have equal voltages $V_+ = V_-$, the maximum voltage is $V_0 = 2V_+$, and $Z_0 = (V_0/2)^2/2P^+ = \pi V_0^2 v/4\omega W_t v_g$.

The following general relation holds at a port of a cavity at resonance [16]: $W_t = (V^2/4)(dB/d\omega)$. In the case of the $\lambda'/2$ resonant slot, we shall assume the port to be at the iris plane $z = 0$ in Fig. 8. We shall set B equal to the total waveguide susceptance B_t at that plane and V equal to the slot voltage V_0 at $x = \lambda'/4$. These choices of B and V are consistent with the waveguide impedance and slot impedance definitions, both of which are on a voltage power basis. Therefore,

$$Z_0 = \frac{\pi}{\omega(dB_t/d\omega)} \cdot \frac{v}{v_g} \quad (62)$$

where $dB_t/d\omega$ is evaluated at the resonant frequency; that is, at $B_t = 0$. Let $\omega = 2\pi c/\lambda$ and $p = \lambda/2a$. Then $\omega = \pi c/ap$ and $d\omega = -(\pi c/ap^2)dp = -\omega(dp/p)$. Substitution of these relations in (62) yields (21).

The ratio v/v_g will now be evaluated. Phase and group velocity are given by $v = \omega/\beta_x = f\lambda'$ and $v_g = d\omega/d\beta_x$ [16], [17] where β_x is the slot-wave phase constant. Since $\beta_x = 2\pi/\lambda'$, we obtain $v_g = -\lambda'^2/(d\lambda'/df)$. Differentiate λ'/λ as follows:

$$\frac{d(\lambda'/\lambda)}{df} = \frac{1}{\lambda}\frac{d\lambda'}{df} - \frac{\lambda'}{\lambda^2}\frac{d\lambda}{df}.$$

Solve this for $d\lambda'/df$ and substitute $d\lambda/df = d(c/f)/df = -\lambda/f$. The resulting relations yield the first part of (20). The second part is obtained in a similar manner.

Acknowledgment

The author wishes to thank E. G. Cristal of Stanford Research Institute for preparing the computer program of the second-order solution, and J. P. Agrios, C. Heinzman and E. A. Mariani of U. S. Army Electronics Command for their experimental studies of slot line. The above people, and also L. A. Robinson and L. Young of Stanford Research Institute, participated in numerous discussions with the author.

References

[1] H. Jasik, Ed., *Antenna Engineering Handbook*. New York: McGraw-Hill, 1961, chs. 8, 9.

[2] A. F. Harvey, *Microwave Engineering*. New York: Academic Press, 1963, pp. 633–638.

[3] W. H. Watson, *Waveguide Transmission and Antenna Systems*. New York: Oxford University Press, 1947.

[4] E. Strumwasser, J. A. Short, R. J. Stegen, and J. R. Miller, "Slot study in rectangular TEM transmission line," Hughes Aircraft Company, Tech. Memo 265, Air Force Contract AF 19(122)-454, January 1952.

[5] M. C. Bailey, "Design of dielectric-covered resonant slots in a rectangular waveguide," *IEEE Trans. Antennas and Propagation*, vol. AP-15, pp. 594–598, September 1967.

[6] J. Galejs, "Excitation of slots in a conducting screen above a lossy dielectric half space," *IRE Trans. Antennas and Propagation*, vol. AP-10, pp. 436–443, July 1962.

[7] S. Ramo and J. R. Whinnery, *Fields and Waves in Modern Radio*, 2nd ed. New York: Wiley, 1953, pp. 357–358.

[8] E. Jahnke and F. Emde, *Tables of Functions with Formulae and Curves*. New York: Dover, 1943, pp. 236–243.

[9] S. B. Cohn, "A theoretical and experimental study of a waveguide filter structure," Cruft Lab., Harvard University, Cambridge, Mass., Tech. Rept. 39, Contract N5 ORI-76, Task Order 1, April 25, 1948.

[10] ——, "Analysis of a wide-band waveguide filter," *Proc. IRE*, vol. 37, pp. 651–656, June 1949.

[11] W. C. Hahn, "A new method for the calculation of cavity resonators," *J. Appl. Phys.*, vol. 12, p. 62, 1941.

[12] J. R. Whinnery and H. W. Jamieson, "Equivalent circuits for discontinuities in transmission lines," *Proc. IRE*, vol. 32, pp. 98–115, February 1944.

[13] S. A. Schelkunoff, *Electromagnetic Waves*. Princeton, N. J.: Van Nostrand, 1943.

[14] N. Marcuvitz, *Waveguide Handbook*, M.I.T. Rad. Lab. Ser., vol. 10. New York: McGraw-Hill, 1951, pp. 218–219.

[15] R. E. Collin, *Field Theory of Guided Waves*. New York: McGraw-Hill, 1960. Use $\Sigma_{1,2,3,\ldots} e^{inx}/n^3$ on p. 579 and $\Sigma_{1,3,5,\ldots} e^{inx}/n^3$ on p. 580.

[16] C. G. Montgomery, R. H. Dicke, and E. M. Purcell, *Principles of Microwave Circuits*, M.I.T. Rad. Lab. Ser., vol. 8. New York: McGraw-Hill, 1948. See p. 230, eq. (40) for relation between W_t, V, and $dB_t/d\omega$; see p. 53, eqs. (103) and (104) for v and v_g.

[17] L. Brillouin, *Wave Propagation in Periodic Structures*. New York: Dover, 1953, pp. 72–76.

[18] F. Oberhettinger and W. Magnus, *Anwendung der Elliptischen Funktionen in Physik und Technik*. Berlin: Springer, 1949, pp. 63, 114–116.

[19] E. Mariani, C. Heinzman, J. Agrios, and S. B. Cohn, "Measurement of slot-line characteristics," presented at the 1969 IEEE G-MTT Internatl. Symp., Dallas, Tex., May 5–7, 1969, to be published in *IEEE Trans. Microwave Theory and Techniques*.

[20] G. H. Robinson and J. L. Allen, "Applications of slot line to miniature ferrite devices," presented at the 1969 IEEE G-MTT Internatl. Symp., Dallas, Tex., May 5–7, 1969.

Current Distribution in Barretters and Its Application to Microwave Power Measurements

JOHN W. ADAMS AND STEPHEN JARVIS, JR.

Abstract—**This paper describes a mathematical analysis for determining the microwave current distribution in a barretter in a rectangular waveguide. This distribution, when used with another analysis which calculates substitution error for any given current distribution, provides a missing step necessary for the calibration of microwave and millimeter-wave barretters for absolute power measurements.**

Manuscript received February 28, 1969; revised May 27, 1969.

J. W. Adams is with the Radio Standards Engineering Division, National Bureau of Standards, Boulder, Colo. 80302.

S. Jarvis is with the Radio Standards Physics Division, National Bureau of Standards, Boulder, Colo. 80302.

I. Introduction

THIS PAPER describes a mathematical analysis of the microwave current distribution in a barretter in a rectangular waveguide. The distribution is determined from an infinite set of linear equations, and a program has been written to evaluate a truncated set. This distribution is of interest in itself but is used here in conjunction with a previous program which calculates substitution error for any given current distribution [1]. The combination of programs when used with efficiency data obtained by microwave techniques [2] will be useful in calibrating barretters for micro-